Movies 1 and 2. Time-lapse images of *mug28Δ* GFP-Psy1 (movie 1) and *mug28*$^{+}$ GFP-Psy1 (movie 2) cells in live meiotic cells. Cells were observed from metaphase II to anaphase II. Images are recorded at 3 minute intervals.

Movies 3 and 4. Time-lapse images of *mug28Δ* Meu14-GFP (movie 3) and *mug28*$^{+}$ Meu14-GFP (movie 4) in live meiotic cells. Cells were observed from metaphase II to anaphase II. Images are recorded at 3 minute intervals.

Movies 5 and 6. Time-lapse images of *mug28Δ* Meu14-GFP GFP-Psy1 (movie 5) and *mug28*$^{+}$ Meu14-GFP GFP-Psy1 (movie 6) in live meiotic cells. Cells were observed from metaphase II to anaphase II. Images are recorded at 3 minute intervals.

Mug28, a meiosis-specific protein of *Schizosaccharomyces pombe*, regulates spore wall formation

Akira Shigehisa, Daisuke Okuzaki, Takashi Kasama, Hideki Tohda, Aiko Hirata and Hiroshi Nojima

SUPPLEMENTARY DATA

SUPPLEMENTARY MATERIALS AND METHODS

Live Cell Observation

To detect Mug28-GFP, Meu10-GFP, and mCherry-Psy1 in living meiotic cells, mid-log-phase *mug28*$^{+}$*-GFP* (AS181) and *meu10*$^{+}$*-GFP mCherry-psy1*$^{+}$ (NP250 and 251) cells were cultured in EMM2-N medium to induce meiosis as described previously (Saito *et al*., 2005). The living cells were then stained with 3.0 μg/ml Hoechst33342 for 5 min and spotted on a coverslip. Fluorescence images of these cells were observed using a fluorescence microscope (BX51; Olympus, Tokyo, Japan) with a Cool SNAP charge-coupled-device camera (Roper Scientific, San Diego, CA). Fluorescence images were acquired using Adobe Photoshop 7.0.

Gene Disruption of mug28^{+}

To disrupt the *mug28*$^{+}$ gene by replacing it with the *ura4*$^{+}$ gene, we used the polymerase chain reaction (PCR) to amplify a DNA fragment carrying the 5' upstream and 3' downstream regions of the *mug28*$^{+}$ gene. For this purpose, we synthesized the following four oligonucleotides and used them as primers (see Table S2 for their sequences): mug28-5'Fw-*Kpn*I, mug28-5'Rv-*Xho*I, mug28-3'Fw-*Xho*I-stop-*Pst*I and mug28-3'Rv-*Sac*I'. These PCR products and the 1.8 kb *Hin*dIII fragment containing the *ura4*$^{+}$ gene were inserted into the pBluescriptII KS (+) vector via *Kpn*I-*Xho*I, *Pst*I-*Sac*I or *Hin*dIII sites. The mug28-5'Fw-*Kpn*I and mug28-3'Rv-*Sac*I primers generated a 2.8 kb PCR product containing the *ura4*$^{+}$ cassette. This plasmid construct was digested with *Kpn*I and *Sac*I, and the resulting construct was introduced into the h^{90} wild-type strain AS6 (*h*^{90} *ade6-M210 leu1-32 ura4-D18*). The Ura^{+} transformants were then screened by PCR analysis to identify the disrupted strain.

Western Blot Analysis

For western blot analysis, 2.8×10^8 *S. pombe* cells were suspended in 0.4 ml of 20% trichloracetic acid (TCA) solution. The cells were disrupted with acid-washed glass beads using a vortex mixer, and then a 5% TCA solution was added and the total protein precipitates were obtained by centrifugation. The protein precipitate was then separated by sodium dodecyl sulfate-polyacrylamide gel electrophoresis (SDS-PAGE), and transferred onto a polyvinylidene difluoride membrane (Immobilon, Millipore, Bedford, MA). These blots were probed with a rat anti-HA polyclonal antibody and the bands were visualized using the Renaissance chemiluminescence system (NEN Life Science, Boston, MA).

Thin-section Electron Microscopy (EM) Observations

Cells were incubated on ME plates at 28°C for 18 h, collected, mounted in a thin layer on a copper grid, and immersed in liquid propane cooled with liquid nitrogen (Leica EM CPC; Leica Microsystems, Vienna, Austria). The frozen cells were transferred to 2% OsO_4 in dry acetone and kept at −80°C for three days. Thereafter, they were gradually warmed from −80°C to 0°C over 5 h, held for 1 h at 0°C, and then warmed from 0°C to 23°C (room temperature) for 2 h (Leica EM AFS; Leica Microsystems). After being washed with dry acetone three times, the samples were infiltrated with increasing concentrations of Spurr's resin in dry acetone and finally with 100% Spurr's resin. After polymerization, ultrathin sections were cut by an ultramicrotome (Leica Ultracut UCT; Leica Microsystems) and stained with uranyl acetate and lead citrate. The sections were viewed on an electron microscope (H-7600; Hitachi Co., Tokyo, Japan) at 100 kV.

Spore wall thickness was measured at five, five, five and ten places (n=25) for four independent *mug28*$^+$ spore walls (see Figures 7F and S7), and their average value was calculated (see Figure 7G). Similarly, spore wall thickness was measured at seven, seven, eight, and nine places (n=31) for four independent *mug28Δ* spore walls (see Figures 7F and S7), and their average value was calculated (see Figure 7G).

Construction of Mug28 Mutants

For efficient construction of various deletion mutants, we first prepared a DNA fragment named 5'UTR+ *mug28*$^+$ORF(1-30)+*Sal*I by PCR that contains the 5'UTR and open reading frame (ORF) of *mug28*$^+$ (1-30) with the *Sal*I site at its 3' end, using the 5'UTR-Fw-*Kpn*I and the inORF-plus-*Sal*I-Rv primers (Table S2). Similarly, we prepared the *Sal*I+ *mug28*$^+$ORF(31-1149) fragment by PCR using inORF-plus-*Sal*I-Fw and inORF-*Bam*HI-Rv primers harboring the *Kpn*I, *Sal*I and *Bam*HI sites (Table S2).

Then, plasmid DNA harboring the 5'UTR+*mug28*$^+$ORF(1-30)+*Sal*I fragment was digested with *Kpn*I/*Sal*I, and the liberated fragment was ligated with the *Sal*I+*mug28*$^+$ ORF(31-1149) fragment to generate the pT7Blue5'UTR+*mug28*$^+$ ORF(1-30)+*Sal*I+*mug28*$^+$ORF(31-1149) fragment. This fragment was subsequently ligated to the *mug28*$^+$ ORF (1149-)-*gfp*-3'UTR fragment that was *Bam*HI/*Sac*I digested from plasmid pBleuScriptII KS(+)+*Ura4*$^+$+*mug28*$^+$ORF(-*Eco*RI 772)-*gfp*-3'UTR, which was used to prepare the AS108 (*h*^{90} *ade6-M210 leu1-32 ura4-D18 mug28*$^+$*::mug28*$^+$*-gfp*) strain. Then, the generated pT7Blue +5'UTR+*mug28*$^+$ORF(+*Sal*I)-*gfp*-3'UTR was digested with *Kpn*I/*Sac*I to release the 5'UTR+*mug28*$^+$ ORF(+*Sal*I)-*gfp*-3'UTR fragment, which was inserted into pJK148 to obtain the basic plasmid, pJK148 5'UTR+*mug28*$^+$ORF(+*Sal*I)-*gfp*-3'UTR, for deletion of mutants-GFP.

To prepare the RRM1Δ strain, we performed PCR with the 5'UTR-Fw-*Kpn*I and the RRM1Δ-*Spe*I-Rv primers (Table S2), using the basic plasmid as a substrate. The generated DNA fragment was digested with *Kpn*I/*Spe*I to obtain the RRM1Δ fragment, which replaced the RRM1 region of the basic Mug28 construct. For RRM2Δ, we performed PCR using the inORF-plus-*Sal*I-Fw (described above) and the RRM2Δ-*Bam*HI-Rv primers harboring the *Bam*HI site (Table S2). The *Sal*I/*Bam*HI digest of the amplification product replaced the RRM2 region of the basic Mug28 construct. For RRM3Δ, the inORF-plus-*Sal*I-Fw primer (described above) and RRM3Δ-*Not*I-Rv primer, harboring the *Not*I site, were used for PCR amplification, and the amplification product was digested with *Sal*I/*Not*I to replace the RRM3 region of the basic Mug28 construct. For RRM1ΔRRM2Δ, the RRM3O-*Sal*I-Fw primer, with the *Sal*I site underlined, and the mug28ORF-3'Rv-*Not*I (nonstop codon) primer (described above) were used for PCR amplification, and the amplification product was digested with *Sal*I/*Not*I for replacement of the RRM1/RRM3 region of the basic Mug28 construct. For RRM2ΔRRM3Δ, the inORF-plus-*Sal*I-Fw primer (described above) and the RRM1O-*Not*I-Rv primer (Table S2). For RRM1ΔRRM3Δ, the RRM2O-*Sal*I-Fw and RRM3Δ-*Not*I-Rv primers harboring the *Not*I, *Sal*I, and *Not*I sites (Table S2), were used for PCR amplification, and the amplification products were digested with *Sal*I/*Not*I to replace the RRM1/RRM3 region of the basic Mug28 construct. Subsequently, these constructs were digested with *Nru*I and introduced into AS99 (*h*^{90} *ade6-M210 leu1-32 ura4-D18 mug28*$^+$*::ura4*$^+$). We screened the Leu$^+$ transformants and confirmed the precise integration of constructs by PCR and digestion with relevant restriction enzymes.

To prepare the Mug28F466A-GFP strain, we synthesized a *mug28*$^+$ORF fragment

harboring the *Bam*HI and *Not*I sites. Then, the plasmid named pJK148 5'UTR+*mug28*$^{+}$ORF(+*Sal*I)-*gfp*-3'UTR was digested with *Bam*HI/*Not*I, and the liberated fragment was exchanged with the *Bam*HI+*mug28*$^{+}$F466A fragment to generate the pJK148 5'UTR+*mug28F466A* ORF(+*Sal*I)-*gfp*-3'UTR plasmid. Subsequently, these constructs were digested with *Nru*I and introduced into AS99 (*h*^{90} *ade6-M210 leu1-32 ura4-D18 mug28*$^{+}$*::ura4*$^{+}$). Then, we screened the Leu^{+} transformants and confirmed the precise integration of the constructs by PCR and digestion mapping with relevant restriction enzymes.

We also prepared 3HA-tagged deletion mutants using a similar process. Briefly, the GFP-*mug28*$^{+}$3'UTR fragment was digested with *Not*I/*Sac*I from the plasmid used for eachmutant-GFP construct and exchanged with the 3HA-*mug28*$^{+}$3'UTR fragment of the pREP41-3HA-*mug28*$^{+}$ 3'UTR plasmid. Then, we obtained the HA-basic plasmid, pJK148 5'UTR+*mug28*$^{+}$ORF(+*Sal*I)-*3ha*-3'UTR, and constructed the 3HA-tagged deletion mutants. Subsequently, these constructs were digested with *Nru*I and introduced into AS99 (*h*^{90} *ade6-M210 leu1-32 ura4-D18 mug28*$^{+}$*::ura4*$^{+}$). Then, we screened the Leu^{+} transformants and confirmed the precise integration of constructs by measuring the size of the DNA fragments that were generated by PCR amplification and subsequent digestion with relevant restriction enzymes. We mated these mutant 3HA-tagged strains with AS193 (*h*$^{+}$ *ade6<<YFP-psy1 his2 leu1-32 ura4-D18*), screened for Ade^{+} transformants and established the mutant strains.

Spore Viability

Spore viability was determined as described previously (Kasama *et al*., 2006). Briefly, haploid parental strains were grown on YPD plates at 33°C. Cells were then mated and sporulated on SPA plates at 28°C (which promoted zygotic meiosis). After three to four days of incubation, the spores were treated with 1% glusulase (PerkinElmer Life Science, Inc.) for 3 h at room temperature and examined under a microscope for complete digestion of contaminating vegetative cells. The glusulase-treated spores were then washed with water and used to measure spore viability. The spores were separated on YPD agar plates using a micromanipulator (Singer Instruments, Somerset, UK). The plates were incubated at 33°C for three days before spore viability was measured.

Construction of the Meu14DD-GFP Strain and Site-directed Mutagenesis

To construct the Meu14DD-GFP mutant strain, the conserved Arg and Leu within two putative destruction boxes (RxxL) of Meu14-GFP were substituted by alanine by site-directed mutagenesis using PCR overlap extension (Weisman and Choder, 2001).

This generated plasmids expressing 5'UTR^{+}-*meu14DD-gfp*-3'UTR with alanine substitutions at R148, L151, R161 and L164. Briefly, the pNP-*meu14*$^{+}$-3'UTR plasmid served as a template in a PCR reaction using the primer pair FN and D1-uncode (5'-CGCTCGTTGTGCATGTGCTCGTGAGGGTGCGAT-3'), and the primer pair D1-code (5'-CACGAGCAGATGCACAACGAGCGATCTCAAGCATTG-3') and FC that contained the R148AL151A mutations. The resulting PCR product was purified by agarose gel electrophoresis (AGE) and used as a template for a second round of PCR with the primer pair FN and FC. Next, the resulting ORF of the meu14 PCR product with two alanine substitutions was purified by AGE and used as a template with primers FN and D2-uncode (5'-CGCAGGATCTGCTTCCTCCTCACGTTCAATGCT-3') and primers D2-code (5'-GTGAGGAGGAAGCAGATCCTGCGTCTCCTAAACTTAC-3') and FC that contained the R161AL164A mutations. The pNP-*meu14*$^{+}$-3'UTR plasmid was replaced by this PCR fragment *via* *Nde*I and *Not*I sites. The resulting *meu14DD-gfp* DNA fragment carrying about 1 kb of both the upstream and downstream regions of *meu14DD* was digested with *Pst*I and *Kpn*I, and then used to transform *meu14*$^{+}$*::ura4*$^{+}$ cells (YDO100). Ura^{-} transformants were obtained from the cells selected on 5-Fruoroorotic Acid (5-FOA) medium and confirmed by Southern blot analysis (data not shown). After confirming the mutations by DNA sequence analysis, we crossed the Meu14DD strain with the GFP-psy1^{+} strain (YN68) to make GFP observations (Figure S6).

DNA Microarray Analysis

Meiotic cells were collected at each time point (0, 4 and 8h) after nitrogen starvation. For monitoring the meiotic expression profiles of *pat1* and *pat1mug28Δ* cells, DNA microarrays constructed by ASPEX corporation (Kanagawa, Japan) were used as described previously (Sugino *et al*., 2009). For each experiment, 50 μg of total RNA was converted into either Cy3- (wild type and *mug28Δ* cells at 0 h) or Cy5- (wild type and mug28Δ cells at 4 h and 8 h) labeled cDNA using a reverse transcriptase reaction kit (TaKaRa Bio Co. Ltd., Ohtsu, Japan) with oligo-dT as the primer. Microarray analysis were performed based on two-color experiments, namely, RNA from cells at 0 h time point was labeled with Cy3, while RNA from meiotic cells at each time point was labeled with Cy5. Hybridized microarrays were scanned for Cy3- and Cy5-labeled targets using a GenePix 4000B scanner (Axon Instruments, Union City, CA) with a resolution of 10 μm. Signal quantification for each probe on the microarray was performed with GenePix acquisition software (version 4.0, Axon Instruments). Clustering and visualization was conducted using GeneSpring GX 10.0.2 (Agilent

technologies).

SUPPLEMENTARY RESULTS

DNA Microarray Analysis of Meiotic mug28Δ Cells

To examine if the RNA binding protein Mug28 has a role in transcriptional regulation, we performed transcriptome analysis of mRNAs from WT and *mug28Δ* cells during meiosis using a homemade DNA microarray of *S. pombe* (Sugino *et al*., 2009). For this purpose, we induced *pat1* (JZ670) and *pat1 mug28Δ* (AS116) cells to enter meiosis synchronously and prepared RNA from cells at 0, 4 and 8 h after meiotic induction (blue arrows in Figure S2A). We compared the mRNA levels at 4 h *vs* 0 h and at 8h *vs* 0 h in each RNA sample by using two-color microarray analysis, which allowed us to obtain a clustered heat map for 3,616 genes out of the 5,130 genes analyzed (Figure S2B-i). The results showed no notable changes in the mRNA levels for most *S. pombe* genes in *mug28Δ* cells during meiosis. Among the genes that were meiotically up-regulated (Figure S2B-ii) or down-regulated (Figure S2B-iii) in *mug28Δ* cells compared to *mug28*$^{+}$ cells, an uncharacterized gene termed *meu6*$^{+}$ (green arrow) showed the most conspicuous difference in expression. Other known meiotically induced genes (Figure S2B-iv) or those tagged with the gene ontology term "expressed during meiosis" in the *S. pombe* Gene DB (Figure S2B-v) did not show a more conspicuous difference in expression than *meu6*$^{+}$ (green arrow). Previously reported spore wall related genes (Figure S2B-vi) or those tagged with the gene ontology term "ascospore-type prospore formation" in the *S. pombe* Gene DB (Figure S2B-vii) also failed to show a more conspicuous difference in expression. The entire processed data sets and each fold change value (Figures S2B and S2C) are presented in Table S3. As for *the meu14*$^{+}$ gene (red arrow), the mRNA level of this gene was slightly higher than in the WT at 4 h, but this difference had almost disappeared at 8 h (Figure S2C). Thus, the residual Meu14-GFP signal (Figures 4 and 5) and Meu14-GFP proteins (Figure 4E) in *mug28Δ* cells were not due to the reduced mRNA level of *meu14*$^{+}$. Since expression of *meu6*$^{+}$ is upregulated at the late stage of meiosis (Watanabe *et al*., 2001), and its expression is largely induced only in *mug28Δ* cells, its function will be analyzed in a future study.

Over-expression of Meu14 Failed to Mimic the Phenotype of mug28Δ Cells

To examine if the residual amount of Meu14 protein at the tip or neck of the snowman-like FSM observed in *mug28Δ* cells is an underlying cause of the abnormal

phenotype of these cells, we constructed Psy1-GFP strains that over-expressed Meu14-9myc protein under the *nmt1*, *nmt41* or *nmt81* promoter, which enables strong, intermediate or weak expression after 18 h of depletion of thiamine in the medium. We incubated these strains on EMM plates in the presence of thiamine. Then, the colonies were transferred onto an EMM plate without thiamine and a nitrogen source to induce Meu14-9myc expression and meiosis. After 18 h incubation, we observed the Psy1-GFP signals in cells at the sporulation stage, when Meu14-9myc had reached maximum expression. We found that over-expression of Meu14 under these *nmt* promoters generated the snowman-like phenotype in only a very small number of cells (Figure S3B). This indicates that the over-expression of Meu14 alone failed to mimic the phenotype of *mug28Δ* cells.

Phenotype of mug28Δmeu14Δ cells

To examine for a genetic interaction between *mug28*$^{+}$ and *meu14*$^{+}$ genes, we compared the phenotypes of *mug28Δ*, *meu14Δ* and *mug28Δ meu14Δ* cells by observing the morphology of the FSM with Psy1-GFP signals. We found that most of the mother ascospores with a budded or snowman-like morphology in *meu14Δ* and *mug28Δ meu14Δ* cells were deformed (red or yellow arrowheads, respectively), whereas those of *mug28Δ* cells looked round and healthy like WT cells (Figure S4A). Moreover, the frequency of budded or snowman-like morphologies in *meu14Δ* and *mug28Δ meu14Δ* cells was lower than in *mug28Δ* cells (Fig. S4B). Furthermore, the fragmented nuclei detected in *meu14Δ* cells (Okuzaki *et al*., 2003) were not observed in *mug28Δ* cells, and the frequency of fragmented nuclei was not altered in *mug28Δ meu14Δ* cells (red bars in Figure S4B). These results show that the phenotypes of *meu14Δ* and *mug28Δ* cells are different and that these phenotypes do not affect each other, indicating the absence of a genetic interaction between *mug28*$^{+}$ and *meu14*$^{+}$genes in these backgrounds.

Ectopic Expression of Meu14DD Mutant

To examine if the abnormal FSM formation observed in *mug28Δ* cells was due to dysregulation of timely degradation of Meu14 at the end of meiosis, we constructed mutant strains that expressed Meu14DD-GFP proteins (Meu14DD-R148AL151A or -R161AL164A), in which conserved Arg and Leu within the two putative destruction boxes (RxxL) were substituted by Ala, and Psy1-GFP for visualization of FSM. An examination of the behavior of FSMs during meiosis under a fluorescence microscope showed no conspicuous difference between the images of Meu14-GFP Psy1-GFP

(NP234) and Meu14DD-GFP Psy1-GFP (NP230) signals from Meiosis II to the sporulation stage (Figure S6A, left and right panels). Nonetheless, it is notable that Meu14DD-GFP/Psy1-GFP signals at the FSM looked stronger than those of Meu14-GFP/Psy1-GFP at the end of Meiosis II (arrowheads in Figure S6B), which suggests that Meu14DD-GFP degradation was at least partly inhibited by the substitutions in the destruction box. We also found that the diameter of the FSM at maximum size was about 25% smaller on average in NP230 strains than *in* NP234 strains (Figure S6C), although the size of the mature spores were almost the same in both strains (data not shown). The results suggest that degradation of Meu14 is regulated by the ubiquitin-proteasome pathway, and that the ectopic expression of Meu14DD proteins caused abnormal FSM formation at the end of Meiosis II.

SUPPLEMENTARY REFERENCES

Sugino, C., Hirose, M., Tohda, H., Yoshinari, Y., Abe, T., Giga-Hama, Y., Iizuka, R., Shimizu, M., Kidokoro, S., Ishii, N., and Yohda, M. (2009). Characterization of a sHsp of Schizosaccharomyces pombe, SpHsp15.8, and the implication of its functional mechanism by comparison with another sHsp, SpHsp16.0. Proteins *74*, 6-17.

Weisman, R., and Choder, M. (2001). The fission yeast TOR homolog, *tor1*$^{+}$, is required for the response to starvation and other stresses via a conserved serine. J. Biol. Chem. *276*, 7027-7032.

SUPPLEMENTARY FIGURE LEGENDS

Figure S1. Ectopic expression of Mug28-GFP suppressed the abnormal sporulation phenotype of *mug28Δ* cells. (A) Comparison of the spore viability between *mug28*$^{+}$ (AS6), *mug28Δ* (AS99), *mug28*$^{+}$*::mug28*$^{+}$*-GFP* (AS108) and Mug28-GFP (AS164) strains indicates the almost complete suppression of the reduced spore viability in *mug28Δ* (AS99) cells. The data show the averages of three independent experiments with standard errors (error bars). At least 200 spores were measured for each strain. (B) Frequency of cells with normal and abnormal morphologies of these *mug28*$^{+}$ (AS6), *mug28Δ* (AS99), *mug28*$^{+}$*::mug28*$^{+}$*-GFP* (AS108) and Mug28-GFP (AS164) strains at sporulation indicate the almost complete suppression of the appearance of abnormally shaped spores in *mug28Δ* (AS99) cells. (C) Typical fluorescence images of the control strain showing that GFP-tagged Mug28 in the AS164 strain displayed a similar localization as in the *mug28*$^{+}$*::mug28*$^{+}$*-GFP* (AS108) strain during meiosis. Fluorescence from Mug28-GFP was observed at meiosis I and II, after meiotic induction by nitrogen starvation. Fluorescence microscopy images of DNA (blue) and Mug28-GFP (green), together with their merged images. Bar, 10 μm.

Figure S2. DNA microarray analysis revealed the meiotic expression profiling of *S. pombe* genes in *mug28Δ* cells. (A) The *h*$^{-}$*/h*$^{-}$ *pat1-114* (JZ670) and *pat1-114 mug28Δ* (AS116) strains were induced to enter meiosis synchronously. The cells were collected at 0, 4, and 8 h time points and total RNAs were harvested for DNA microarray analysis as 2 color experiments (4/0 hour of JZ670, 8/0 hour of JZ670, 4/0 hour of AS116 and 8/0 hour of AS116). The time points of the collections are indicated by arrows. (B) Heat map analysis. (i) Hierarchical clustering of 3,616 genes is presented using the analytically available data. Rows and columns represent the analyzed genes and their expression profiles in JZ670 and AS116 strains at 4 and 8 h after nitrogen starvation. The $\log_2$ ratio of expression levels at each time point (4 and 8 h) relative to the levels at 0 h are color-coded as indicated at the bottom. (ii) Hierarchical clustering for the meiotically up-regulated genes that showed distinct expression patterns in *mug28Δ* cells compared to *mug28*$^{+}$ cells. (ii) Hierarchical clustering for the meiotically down-regulated genes that showed distinct expression patterns in *mug28Δ* cells compared to *mug28*$^{+}$ cells. (iv) Hierarchical clustering of 19 *meu* genes that were identified previously (Watanabe *et al*., 2001). (v) Hierarchical clustering of 6 genes whose products are associated with the 'expressed during meiosis' term in the Sz. pombe GeneDB (http://www.genedb.org/genedb/pombe/). (vi) Hierarchical

clustering of 9 genes whose products are associated with the 'ascospore-type prospore formation' term in the DB. (C) Bar graph indicates the expression levels of *meu14*$^{+}$, *meu6*$^{+}$, *leu1*$^{+}$ and *atb2*$^{+}$ genes; the y axis shows the fold-change relative to the 0 h time point. The *leu1*$^{+}$ and *atb2*$^{+}$ genes are shown as low level expression controls to compare the bar graph impression with that of heat map.

Figure S3. Microscopic visualization of Meu10-GFP and FSM formation. (A) Subcellular localization of Meu10-GFP in living NP250 (*h*^{90} *meu10*$^{+}$*-GFP mCherry-psy1*$^{+}$: i) and NP251 (*h*^{90} *meu10*$^{+}$*-GFP mCherry-psy1*$^{+}$ *mug28*$^{+}$*::ura4*$^{+}$: ii-iv) cells. Fluorescence signals from Meu10-GFP were observed during sporulation after meiotic induction by nitrogen starvation. Fluorescence microscopy images of DNA (blue), mCherry-Psy1 (red), and Meu10-GFP (green) are shown. White arrowheads denote Meu10-GFP localized to deformed mother ascospores displaying budded or snowman-like morphology. Bar, 10 μm. (B) FSM formation in *psy1-GFP* strains (FY12104) ectopically expressing Meu14-9myc under various *nmt* promoters. Psy1-GFP cells harboring pRmM1, pRmM41, or pRmM81 plasmids (*meu14*$^{+}$*-9myc* driven by the *nmt1*, *nmt41* and *nmt81* promoters, respectively) were meiotically induced on sporulation plates without thiamine for ectopic expression at 30°C for 18 h. Psy1 localization in each strain was classified into three groups: normal (a), budded (b), and snowman-like (c). At least 250 spores were measured.

Figure S4. Abnormal phenotypes were observed in Psy1-GFP in *mug28Δmeu14Δ* double mutant cells. (A) GFP-Psy1 dynamics and nuclei in cells from meiosis II to sporulation are shown in wild type (YN68; i-ii), *meu14Δ* (NP226; iii-v), *mug28Δ* (AS117; vi-vii) and *mug28Δmeu14Δ* (NP230; viii-x) cells harboring *psy1*$^{+}$*-GFP*. Cells were induced to enter meiosis at 28°C for 2 days, and then stained with Hoechst33342 (0.5 μg/ml) for nuclear visualization. Psy1-GFP (green), nucleus (DNA; blue) and their merged images are shown. Red or yellow arrowheads denote the deformed mother ascospores harboring budded or snowman-like patterns. Bar, 10 μm. (B) The histogram shows the percentage of normal and abnormal cells expressing Psy1-GFP in wild type (YN68), *meu14Δ* (NP226), *mug28Δ* (AS117) and *mug28Δmeu14Δ* (NP230) cells. Images are classified as class I (meiotic nuclei are fragmented), class II (FSMs are encapsulated into four nuclei), class III (Psy1-GFP show budded appearance), class IV (Psy1-GFP show snowman-like appearance) and class V (other phenotypes). At least 100 cells were counted.

Figure S5. Time-lapse images of FSM formation and/or the leading edge protein behavior in *mug28*$^{+}$ (YN68, YOD50, SOP091w) cells at 28°C. GFP images that were captured every 6 min are presented for the YN68 (*GFP-psy1*$^{+}$) strain (A) and the YOD50 (*meu14*$^{+}$*-GFP*) strain (B). GFP images that were captured every 2.5 min are also shown for the SOP091w (*meu14*$^{+}$*-GFP GFP-psy1*$^{+}$) strain (C). Numbers indicated at the bottom of some photographs denote the time, in minutes, from the onset of FSM formation. Scale bars, 10 μm.

Figure S6. Delayed disappearance of Meu14 rings during meiosis is independent on the snowman-like phenotype of the *mug28*Δ strain. (A) A comparison of FSM formation in Meu14-GFP (NP234: wild type) and Meu14DD-GFP (NP239: a mutant) cells harboring *psy1*$^{+}$*-gfp*. NP239 cells express Meu14DD-GFP with alanine substitutions at R135, L138, R148 and L151 residues located within the two putative destruction boxes (RxxL motif; see Materials and methods). Cells were meiotically induced on sprulation plates at 28°C for 24 h and stained with Hoechst33342 (0.5 μg/ml) for nuclear visualization. Typical images (DIC, DNA, Meu14-GFP/Psy1-GFP and the merged images) of meiotic Meu14-GFP (left panel) and Meu14DD-GFP (right panel) cells are shown. Bar, 10 μm. (B) Typical images of meiotic Meu14-GFP (NP234) and Meu14DD-GFP (NP239) are shown. Bar, 10 μm. (C) Comparison of the diameter of Meu14 rings between Meu14-GFP and Meu14DD-GFP strains. Three independent strains of Meu14-GFP (NP234, NP235 and NP236) and Meu14DD-GFP (NP239, NP240 and NP241) were collected and the Meu14 ring diameter was measured. A plot of the diameter of the Meu14 ring (y-axis), the independently measured strains (x-axis) and the average values (arrowhead) are shown. Inset shows a schematic presentation of the diameter of the Meu14 ring. Diameters of leading edges were measured using MetaVue 7.5.0.0 software (Molecular Devices, Downingtown, PA).

Figure S7. Typical images of TEM photographs of *mug28*$^{+}$ (AS6) and *mug28Δ* (AS99) spores that were used for the measurement of spore wall thickness. Spore wall thickness was measured at the positions indicated with white bars. Black scale bar, 0.5 μm.

Figure S8. Spore viability of Mug28-GFP (AS164), Mug28-RRM3Δ-GFP (AS175), Mug28-3HA (AS197), and Mug28-RRM3Δ-3HA (AS200) strains. Spore viability was measured by random spore analysis. At least 200 spores were measured.

Figure S9. No genetic interaction was observed between *mug28*$^{+}$ and *sst4*$^{+}$ genes during meiosis. (A) Subcellular localization of Sst4-mRFP in living AS214 (*h*^{90} *sst4*$^{+}$*-mRFP mug28Δ*) cells. Fluorescence signals from Sst4-mRFP were observed at various stages of meiosis after meiotic induction by nitrogen starvation. DIC images are shown in the leftmost panels. DNA (blue), Sst4-mRFP (red) and the corresponding merged images are shown (B) Subcellular localization of Mug28-GFP in living AS217 (*h*^{90} *mug28*$^{+}$*-GFP sst4Δ*) cells. Fluorescence signals from Mug28-GFP were observed at various stages of meiosis after meiotic induction by nitrogen starvation. DIC images are shown in the leftmost panels. DNA (blue), Mug28-GFP (green) and the corresponding merged images are shown. Bar, 10 μm. (C) Spore viability of wild type (AS6), *mug28Δ* (AS99), *sst4Δ* (MI368) and *mug28Δsst4Δ* (AS213) strains. Spore viabilities were measured by random spore analysis. Bar graphs show the averages of three independent experiments with standard errors (error bars). At least 200 spores were measured.

Table S1. Yeast strains used in this study.

Strain name	Genotype	Source/reference
CD16-1	*h^{+}/h^{-} ade6-M210/ade6-M216 cyh1/$^{+}$ $^{+}$/lys5-391*	C. Shimoda
CD16-5	*h^{-}/h^{-} ade6-M210/ade6-M216 cyh1/$^{+}$ $^{+}$/lys5-391*	C. Shimoda
AS6	*h^{90} ade6-M210 leu1-32 ura4-D18*	This study
AS99	*h^{90} ade6-M210 leu1-32 ura4-D18 mug28^{+}::ura4^{+}*	This study
JZ670	*h^{-}/h^{-} ade6-M210/ade6-M216 leu1-32/leu1-32 pat1-114/pat1-114*	M. Yamamoto
AS127	*h^{90} ade6-M210 leu1-32::sad1-mCherry-leu1^{+} ura4-D18 mug28^{+}::mug28^{+}-GFP-ura4^{+}*	This study
YN68	*h^{90} leu1-32<<GFP-psy1^{+}-leu1^{+}*	C. Shimoda
AS117	*h^{90} ade6-M216 leu1-32<<GFP-psy1^{+}-leu1^{+} ura4-D18 mug28^{+}::ura4^{+}*	This study
AS122	*h^{-}/h^{-} ade6-M210/ade6-M216 leu1-32/leu1-32 ura4-D18/ura4D18 pat1-114/pat1-114 mug28^{+}::[mug28^{+}-3HA-ura4^{+}]/mug28^{+}::[mug28^{+}-3HA-ura4^{+}]*	This study
YDO50	*h^{90} leu1-32 ura4-D18 meu14^{+}::meu14^{+}-GFP*	D. Okuzaki
YDO121	*h^{+} ade6-M216 his2 leu1-32 ura4-D18 meu14^{+}::meu14^{+}-GFP spo3^{+}-HA-LEU2^{+}*	D. Okuzaki
AS160	*h^{90} leu1-32 ura4-D18 mug28^{+}::ura4^{+} meu14^{+}::meu14^{+}-GFP*	This study
SOP091w	*h^{90} leu1-32 ura4-D18 leu1<<GFP-psy1^{+} meu14^{+}-GFP*	A. Ohtaka
AS161	*h^{90} ade6-M216 leu1-32::psy1^{+}-GFP-leu1^{+} ura4-D18 mug28^{+}::ura4^{+} meu14^{+}::meu14^{+}-GFP*	This study
AS164	*h^{90} ade6-M210 leu1-32::mug28^{+}-GFP-leu1^{+} ura4-D18 mug28^{+}::ura4^{+}*	This study
AS172	*h^{90} ade6-M210 leu1-32::mug28^{+}-RRM1Δ-GFP-leu1^{+} ura4-D18 mug28^{+}::ura4^{+}*	This study
AS173	*h^{90} ade6-M210 leu1-32::mug28^{+}-RRM2ΔRRM3Δ-GFP-leu1^{+} ura4-D18 mug28^{+}::ura4^{+}*	This study
AS174	*h^{90} ade6-M210 leu1-32::mug28^{+}-RRM2Δ-GFP-leu1^{+} ura4-D18 mug28^{+}::ura4^{+}*	This study
AS175	*h^{90} ade6-M210 leu1-32::mug28^{+}-RRM1ΔRRM3Δ-GFP-leu1^{+} ura4-D18 mug28^{+}::ura4^{+}*	This study
AS176	*h^{90} ade6-M210 leu1-32::mug28^{+}-RRM3Δ-GFP-leu1^{+} ura4-D18 mug28^{+}::ura4^{+}*	This study
AS177	*h^{90} ade6-M210 leu1-32::mug28^{+}-RRM1ΔRRM2Δ-GFP-leu1^{+} ura4-D18 mug28^{+}::ura4^{+}*	This study
AS185	*h^{90} ade6-M210 leu1-32::mug28^{+}-3HA-leu1^{+} ura4-D18 mug28^{+}::ura4^{+}*	This study
FY13203	*h^{90} ade6<<YFP-psy1^{+} leu1-32*	NBRP
AS197	*h^{90} ade6<<YFP-psy1^{+} leu1-32::mug28^{+}-3HA-leu1^{+} ura4-D18 mug28^{+}::ura4^{+}*	This study
AS198	*h^{90} ade6<<YFP-psy1^{+} leu1-32::mug28^{+}-RRM1Δ-3HA-leu1^{+} ura4-D18 mug28^{+}::ura4^{+}*	This study
AS199	*h^{90} ade6<<YFP-psy1^{+} leu1-32::mug28^{+}-RRM2Δ-3HA-leu1^{+} ura4-D18 mug28^{+}::ura4^{+}*	This study

AS200	*h^{90} ade6<<YFP-psy1^{+} leu1-32::mug28^{+}-RRM3Δ-3HA-leu1^{+} ura4-D18 mug28^{+}::ura4^{+}*	This study
AS201	*h^{90} ade6<<YFP-psy1^{+} leu1-32::mug28^{+}-RRM2ΔRRM3Δ-3HA-leu1^{+} ura4-D18 mug28^{+}::ura4^{+}*	This study
AS202	*h^{90} ade6<<YFP-psy1^{+} leu1-32::mug28^{+}-RRM1ΔRRM3Δ-3HA-leu1^{+} ura4-D18 mug28^{+}::ura4^{+}*	This study
AS203	*h^{90} ade6<<YFP-psy1^{+} leu1-32::mug28^{+}-RRM1ΔRRM2Δ-3HA-leu1^{+} ura4-D18 mug28^{+}::ura4^{+}*	This study
AS116	*h^{-}/h^{-} ade6-M210/ade6-M216 leu1-32/leu1-32 pat1-114/pat1-114 mug28^{+}::ura4^{+}/ mug28^{+}::ura4^{+}*	This study
FY12104	*h^{90} ade6<<GFP-psy1^{+} leu1-32*	NBRP
NP234	*h^{90} ade6<<psy1^{+}-GFP meu14^{+}-GFP leu1-32 ura4-D18*	This study
NP235	the parent strain of NP234 strain	This study
NP236	the parent strain of NP234 strain	This study
NP239	*h^{90} ade6<<psy1^{+}-GFP meu14DD-GFP leu1-32 ura4-D18*	This study
NP240	the parent strain of NP239 strain	This study
NP241	the parent strain of NP239 strain	This study
NP226	*h^{90} ade6-M216 ura4-D18 leu1<<GFP-psy1^{+} meu14^{+}::ura4^{+}*	This study
NP230	*h^{90} ade6-M216 ura4-D18 leu1<<GFP-psy1^{+} meu14^{+}::ura4^{+} mug28^{+}::ura4^{+}*	This study
TTM101	*h^{-} ade6-M210 ura4-D18 leu1-32 meu10^{+}-GFP*	T. Tougan
NP250	*h^{90} ade6-M210 ura4-D18 leu1-32:mCherry-psy1^{+}-leu1^{+}meu10^{+}-GFP*	This study
NP251	*h^{90} ade6-M210 ura4-D18 leu1-32:mCherry-psy1^{+}-leu1^{+} meu10^{+}-GFP mug28^{+}::ura4^{+}*	This study
NP252	*h^{90} ade6-M210 leu1-32::mug28F466A-GFP-leu1^{+} ura4-D18*	This study
AS181	*h^{90} ade6-M210 leu1-32:: mCherry-psy1^{+}-leu1^{+} ura4-D18 mug28::mug28-GFP-ura4^{+}*	This study

NBRP: National BioResource Project http://yeast.lab.nig.ac.jp/nig/

Table S2. Oligonucleotide primers used in this study

Primer	Sequence
mug28-5'Fw-*Kpn*I	5'-GCGGTACCGAGACAAATATGTAATAAAGGCTGTGTAGT-3'
mug28-5'Rv-*Xho*I	5'-GCCTCGAGTGTGATGTGTCTAGTTGGTAATTATAGAAT-3'
mug28-3'Fw-*Xho*I-stop-*Pst*I	5'-GCCTCGAGTAACTGCAGATAAAAGCAAGATATGTCTAAAGGACATAA-3'
mug28-3'Rv-*Sac*I	5'-GCGAGCTCTTACTCTTTTGGTCACTGGTGGTCTATGAC-3'
mug28-5'Fw-*Asc*I-*Sal*I	5′-GCGGCGCGCCGTCGACGATGATTGCACTTGAAAAACTTTCAG-3′
mug28-3'Rv-*Not*I(non-stop codon)	5′-GCGCGGCCGCCCTTGGTTTAATACAATGTTGGTTAAAGG-3′
5'UTR-Fw-*Kpn*I	5'-CGGGGTACCCTCTACTATAAGAACATCTTGTG-3'
inORF-plus-*Sal*I-Rv	5'-ACGCGTCGACCTTTTCTGAAAGTTTTTCAAGTGCAATCAT-3'
inORF-plus-*Sal*I-Fw	5'-ACGCGTCGACAACAAAAGGAGCACTAAGAAGTGTGAAATT-3'
inORF-*Bam*HI-Rv	5'-GTAAAATGGATCCTTCATACGCAATGGCGTGAAATTTTTC-3'
RRM1Δ-*Spe*I-Rv	5'-GACTAGTGCTCCTTTTGTTGTCGAC-3'
RRM2Δ-*Bam*HI-Rv	5'-GCGGATCCGTACAAAAATTGGGGATTCTGTTCTAGAAGC-3'
RRM3Δ-*Not*I-Rv	5'-GCGCGGCCGCCCCGGTGTTGAGGTTGGTGTTGGCG-3'
RRM3O-*Sal*I-Fw	5'-GCGTCGACCCTGTTCAGGGATTTTGCTCTAATTTG-3'
RRM1O-*Not*I-Rv	5'-GCGCGGCCGCCCAGGGTTGTCGTACAAAAATTGGGG-3'
RRM2O-*Sal*I-Fw	5'-GCGTCGACATCGTGGAGAGATACAAAAATAAGTTGG-3'
RRM3Δ-*Not*I-Rv	5'-GCGCGGCCGCCCCGGTGTTGAGGTTGGTGTTGGCG-3'
D1-coding	5'-CACGAGCAGAT***GCA***CAACGA***GCG***ATCTCAAGCATTG-3'
D2-coding	5'-GTGAGGAGGAA***GCA***GATCCT***GCG***TCTCCTAAACTTAC-3'
D1-noncoding	5'-***CGC***TCGTTG***TGC***ATGTGCTCGTGAGGGTGCGAT-3'
D2-noncoding	5'-***CGC***AGGATC***TGC***TTCCTCCTCACGTTCAATGCT-3'

Restriction enzyme sites are underlined. The codons used for alanine substitutions are denoted by bold italics.

Table S3. Microarray data used to draw Figure S2 were presented below.

(A) Microarray data for Fig. S2C.

	Fold Change			
	mug28+ 4h	*mug28+* 8h	*mug28Δ* 4h	*mug28Δ* 8h
meu14^{+}	80.3	9.1	122.7	6.6
meu6+	7.7	127.2	230.4	356.0
leu1^{+}	-2.4	-1.2	-2.3	-2.8
atb2^{+}	3.3	-1.2	2.5	-1.1

(B) Microarray data for Fig. S2B-ii.

	Fold Change			
	mug28+ 4h	*mug28+* 8h	*mug28Δ* 4h	*mug28Δ* 8h
SPCC1919.05	6.8	1.0	5.3	-3.8
SPBP23A10.03C	3.2	-1.2	4.1	-4.7
rad60^{+}	45.8	1.3	36.8	3.7
chp2^{+}	1.3	-2.8	4.3	-4.2
SPCC1529.01	7.5	-1.4	1.5	-1.9
SPCC645.11C	7.1	1.5	8.9	-5.0
SPBC30D10.07C	6.5	-1.1	6.5	-3.5
sut1^{+}	64.9	4.3	69.7	-1.0
meu6^{+}	7.7	127.2	230.4	356.0
ght3^{+}	16.7	1.3	7.3	-2.7

(C) Microarray data for Fig. S2B-iii.

	Fold Change			
	mug28+ 4h	*mug28+* 8h	*mug28Δ* 4h	*mug28Δ* 8h
aes1^{+}	-19.5	-1.4	-100.0	-38.4
ade8+	-1.4	1.5	-6.0	1.3
SPAC3A11.10C	-3.9	1.8	-9.4	-1.4
SPAC3H8.07C	-5.6	1.2	-4.0	3.2
nog1+	-100.0	-2.0	-8.0	-2.0
SPAC27F1.05C	-3.0	-1.2	-23.4	-6.5
rad50^{+}	-12.6	-4.5	-2.8	-8.1
SPBC14C8.09C	-6.0	1.0	-3.7	3.1

(D) Microarray data for Fig. S2B-iv.

	Fold Change			
	mug28+ 4h	*mug28+* 8h	*mug28Δ* 4h	*mug28Δ* 8h
meu14^{+}	80.3	9.1	122.7	6.6
meu24^{+}	28.5	143.8	18.5	38.5
meu17^{+}	399.3	77.6	413.7	47.9
meu9^{+}	5.7	11.4	9.9	15.6
meu8+	-2.0	-1.2	-7.6	-4.4
meu5^{+}	30.4	108.3	61.4	163.0
meu29^{+}	-1.4	2.3	-1.7	1.8
meu7^{+}	2301.5	851.9	1095.6	434.3
meu18^{+}	31.1	2.3	14.9	5.2
meu25^{+}	102.6	42.8	166.0	20.8
meu12^{+}	75.6	13.3	74.9	16.7
meu28^{+}	45.7	9.2	46.9	5.9
meu21^{+}	37.8	2.3	36.4	2.8
meu5^{+}	340.4	13.8	236.6	4.2
meu30^{+}	-1.3	-1.9	-1.0	-3.0
meu6^{+}	7.7	127.2	230.4	356.0
meu10^{+}	1656.4	91.7	710.5	75.2
meu4^{+}	912.6	1445.6	634.1	460.6
meu27^{+}	67.5	74.6	95.8	89.8

(E) Microarray data for Fig. S2B-v.

	Fold Change			
	mug28+ 4h	*mug28+* 8h	*mug28Δ* 4h	*mug28Δ* 8h
mcp4^{+}	52.0	9.3	76.7	9.6
mcp1^{+}	15.2	2.3	7.8	3.1
mcp^{+}	3.1	1.8	5.4	2.5
cam2^{+}	2.2	1.1	2.5	1.3
spn5^{+}	45.7	9.2	46.9	5.9
mcp5^{+}	5.5	-2.4	7.0	-3.6

(F) Microarray data for Fig. S2B-vi.

	Fold Change			
	mug28+ 4h	*mug28+* 8h	*mug28Δ* 4h	*mug28Δ* 8h
spo3^{+}	161.0	12.5	121.9	20.4
cta4^{+}	1.3	-1.9	1.1	-2.2
spo14^{+}	-2.0	1.2	-2.4	-1.1
meu14^{+}	80.3	9.1	122.7	6.6
spo20^{+}	-1.8	-1.3	-1.9	-1.4
psy1^{+}	5.5	2.1	6.3	2.5
cam2^{+}	2.2	1.1	2.5	1.3
ypt7^{+}	-1.2	1.1	-1.1	1.0
sec9^{+}	3.2	-1.4	4.3	-1.3

(G) Microarray data for Fig. S2B-vii.

	Fold Change			
	mug28+ 4h	*mug28+* 8h	*mug28Δ* 4h	*mug28Δ* 8h
bgs2+	37.8	2.3	36.4	2.8
cam2^{+}	2.2	1.1	2.5	1.3
chs1^{+}	2.3	-2.4	2.5	ND
crp79^{+}(*meu5*$^{+}$)	340.4	13.8	236.6	4.2
acp1^{+}	-3.7	-1.0	-4.2	-1.0
acp2^{+}	1.3	-1.4	1.3	-2.0
myo1^{+}	1.5	1.4	1.1	-1.0
sst4^{+}/ *vsp27*$^{+}$	6.2	2.5	2.6	1.4
spo20^{+}	-1.8	-1.3	-1.9	-1.4

Figure S1. Shigehisa *et al*.

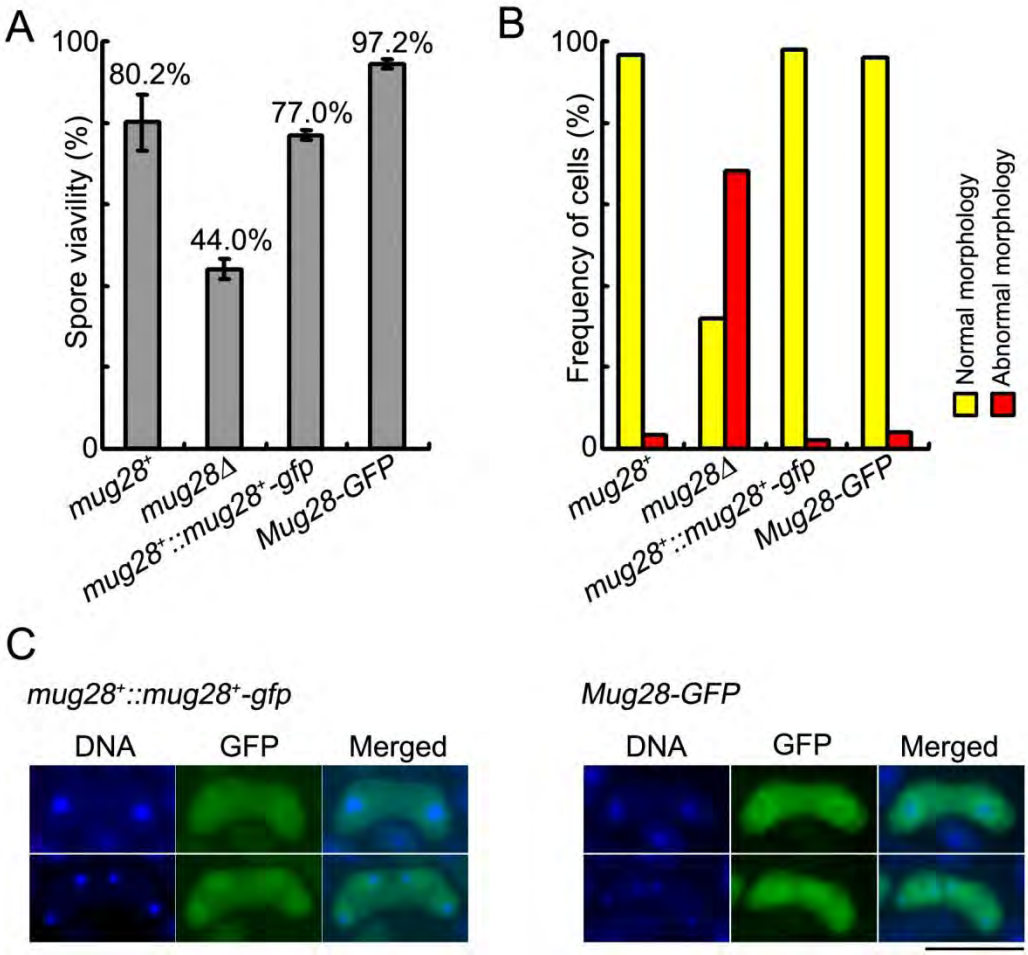

Figure S2. Shigehisa *et al*

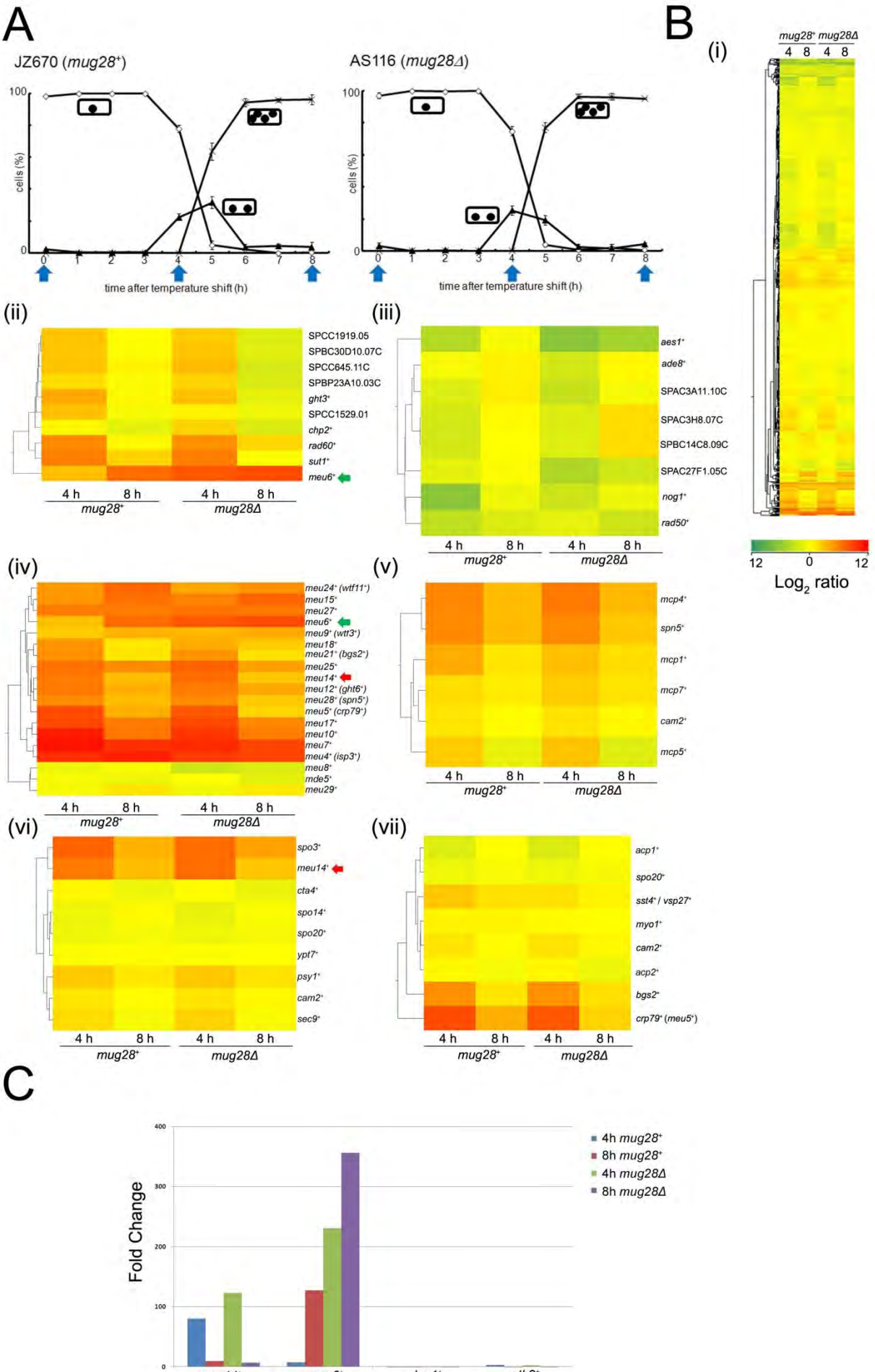

Figure S3. Shigehisa *et al*.

A

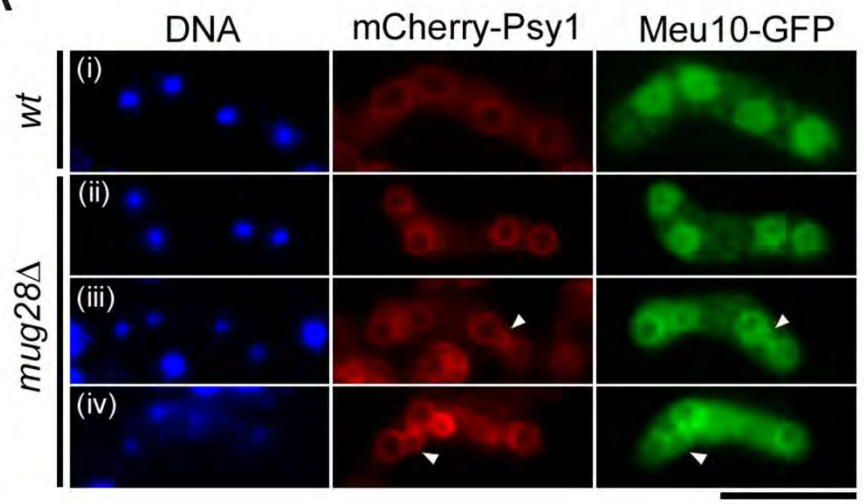

B

Psy1-GFP	*nmt1 meu14⁺-9myc*	*nmt41 meu14⁺-9myc*	*nmt81 meu14⁺-9myc*
a) 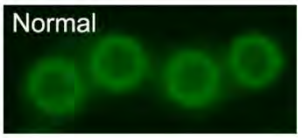 Normal	98.7 % ± 1.1 %	97.9 % ± 2.1 %	97.6 % ± 2.2 %
b) 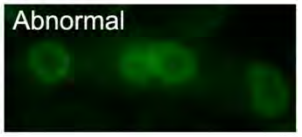 Abnormal	1.1 % ± 1.0 %	2.1 % ± 2.1 %	1.6 % ± 2.2 %
c) 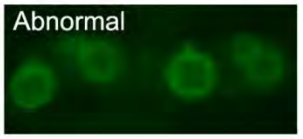 Abnormal	0.2 %± 0.3 %	0.0 %	1.8 %± 1.4 %

Figure S4. Shigehisa *et al*.

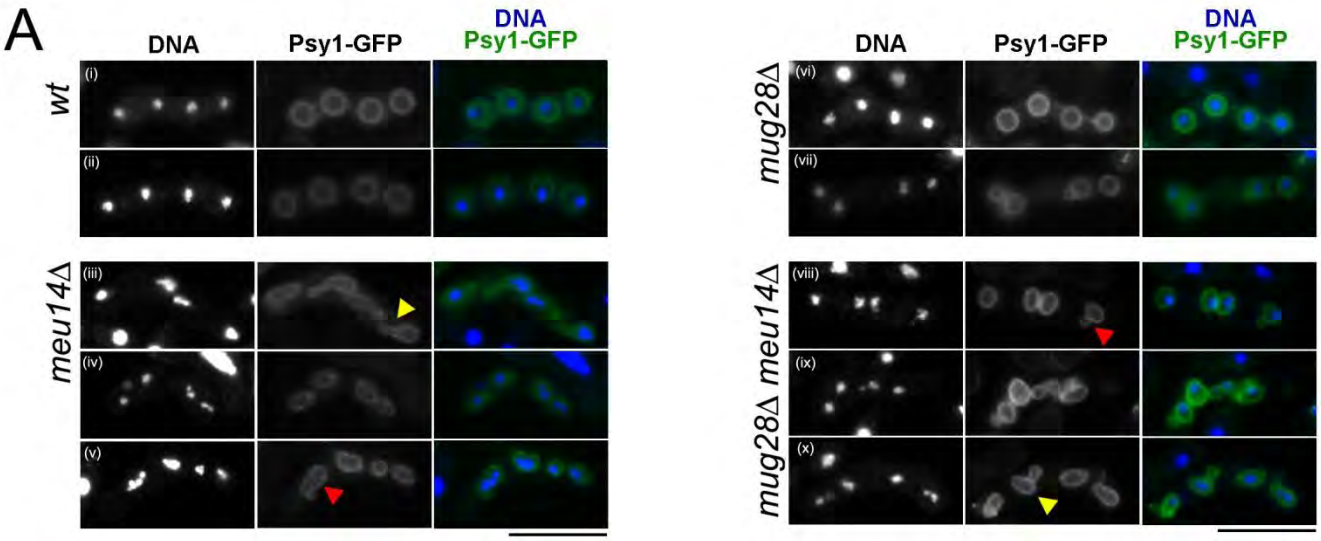

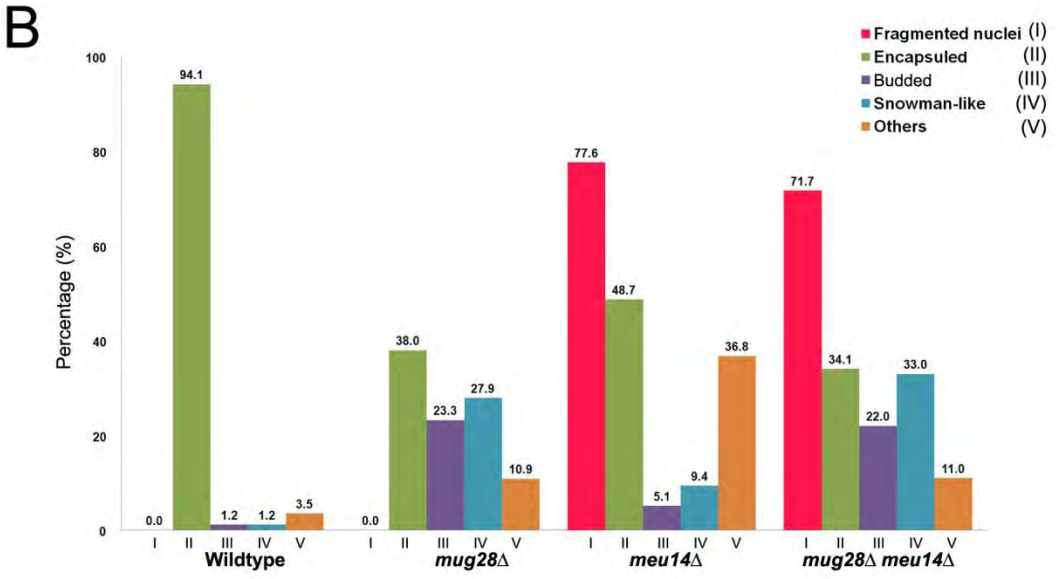

Figure S5. Shigehisa *et al*

A. *mug28*$^{+}$ *GFP-Psy1*

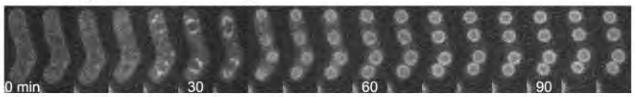

B. *mug28*$^{+}$ *Meu14-GFP*

C. *mug28*$^{+}$ *Meu14-GFP GFP-Psy1*

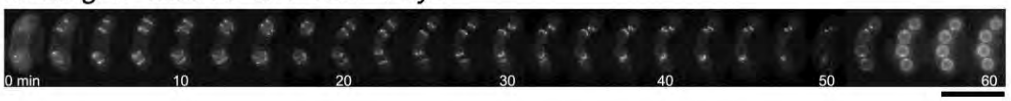

Figure S6. Shigehisa A, *et al*.

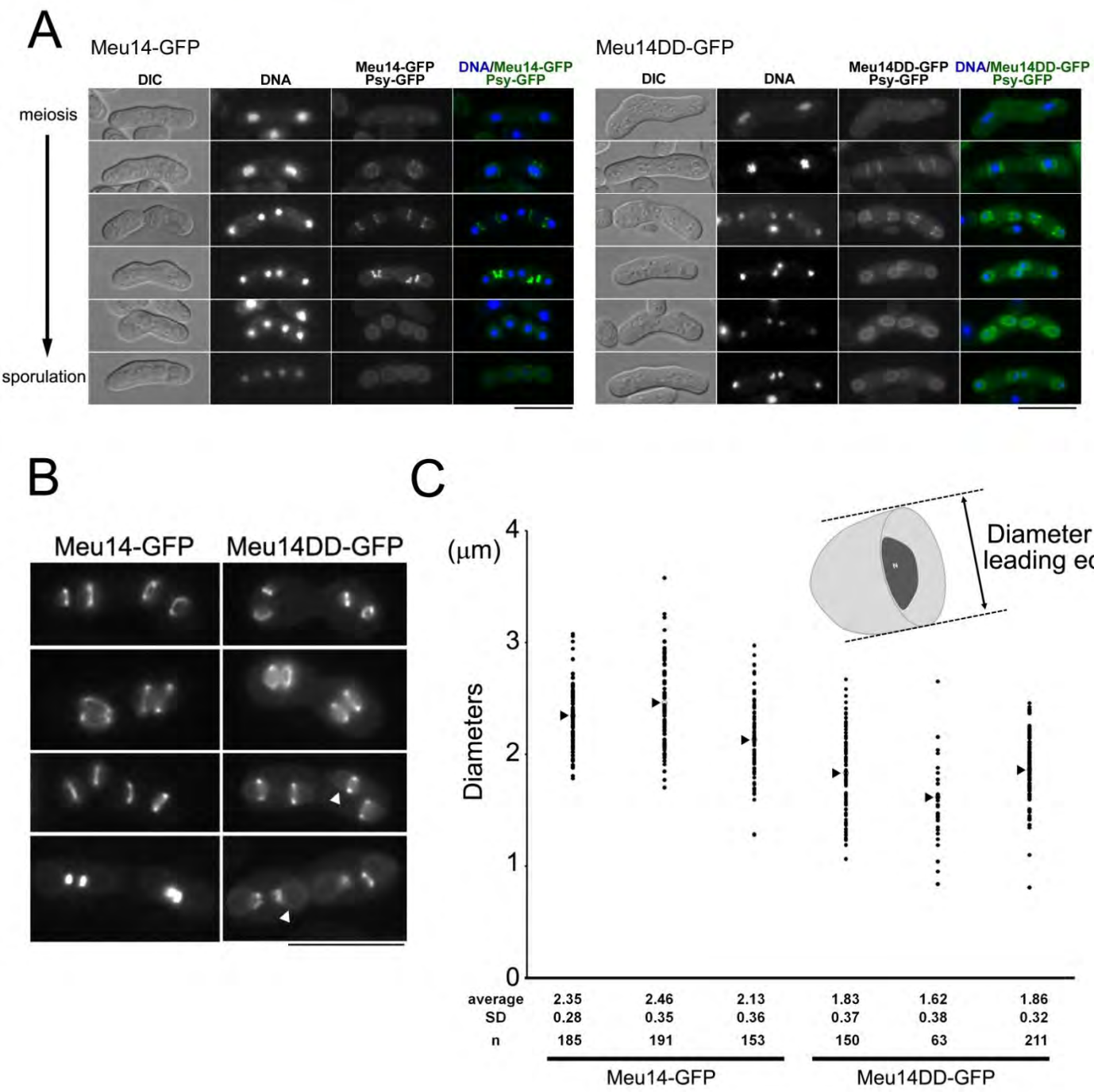

Figure S7. Shigehisa *et al*

mug28^{+}

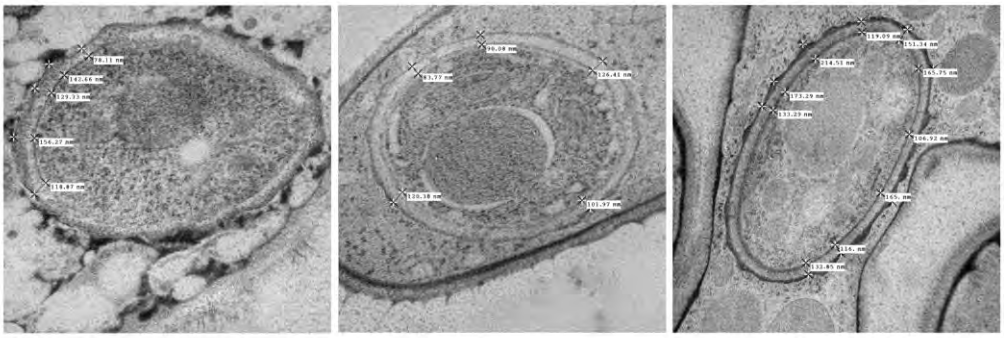

mug28Δ

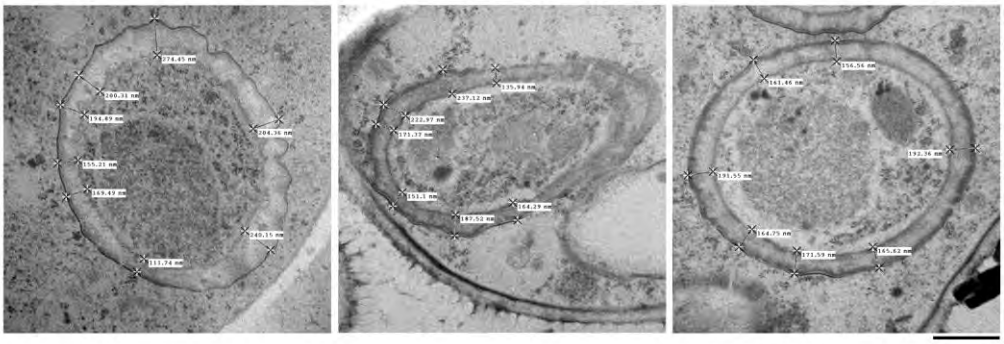

Figure S8. Shigehisa*et al*.

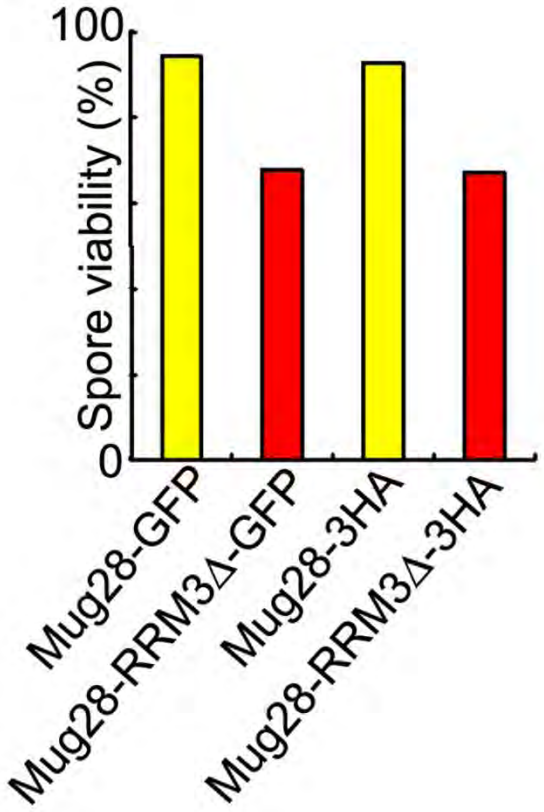

Figure S9. Shigehisa *et al.*